


High-Threshold Quantum Computing by Fusing One-Dimensional Cluster StatesStefano Paesani^{1,2,*} and Benjamin J. Brown^{3,4}¹*Center for Hybrid Quantum Networks (Hy-Q), Niels Bohr Institute, University of Copenhagen, Blegdamsvej 17, Copenhagen 2100, Denmark*²*NNF Quantum Computing Programme, Niels Bohr Institute, University of Copenhagen, Blegdamsvej 17, Copenhagen 2100, Denmark*³*IBM Quantum, T. J. Watson Research Center, Yorktown Heights, New York 10598, USA*⁴*IBM Denmark, Prøvensvej 1, Brøndby 2605, Denmark* (Received 23 December 2022; accepted 11 July 2023; published 21 September 2023)

We propose a measurement-based model for fault-tolerant quantum computation that can be realized with one-dimensional cluster states and fusion measurements only; basic resources that are readily available with scalable photonic hardware. Our simulations demonstrate high thresholds compared with other measurement-based models realized with basic entangled resources and 2-qubit fusion measurements. Its high tolerance to noise indicates that our practical construction offers a promising route to scalable quantum computing with quantum emitters and linear-optical elements.

DOI: [10.1103/PhysRevLett.131.120603](https://doi.org/10.1103/PhysRevLett.131.120603)

Introduction.—Scalable quantum-computing architectures [1,2] are built on quantum error-correcting codes [3] that identify and correct for errors that quantum hardware experiences as logical algorithms progress. However, it remains difficult to produce an architecture with a sufficiently large number of high-quality qubits to complete long quantum computations reliably. To overcome this technological challenge, we should design bespoke quantum architectures that take advantage of the positive features of scalable physical hardware [4–18]. Ideally, we should exploit the native operations of the underlying quantum system to minimize the noise processes that will lead to computational errors.

Quantum emitters are a promising tool to implement photonic architectures [19,20]. They enable the deterministic generation of a variety of entangled states with even a single emitter [21,22], such as one-dimensional cluster states [21,23], via appropriate pulse sequences driving a spin-photon interface interleaved with photon emission. Quantum emitters have been demonstrated with several hardware platforms, including quantum dots [24,25], atomic systems [26,27], superconducting circuits [28], and nitrogen-vacancy centers [29]. Indeed, deterministic entanglement has recently been demonstrated between as many as 14 photons [27].

Measurement-based models for fault-tolerant quantum computing [30] are particularly well suited for photonic

architectures. In this model, we prepare entangled resources that can be produced by constant-depth circuits. Measuring these resources processes quantum information and, at the same time, extracts syndrome data for error correction. We often consider realizing the resource states by entangling individual physical qubits [6,9] or small, constant-sized, entangled resources [7,12]. These proposals place a significant demand on optical hardware to entangle the individual physical systems, using either unitary gates or fusion-based operations [31].

Here, we find that we can reduce the complexity of realizing entangled resources by taking advantage of the one-dimensional entangled states we can produce readily with quantum emitters. The remaining entangling operations that are needed to perform measurement-based fault-tolerant quantum computing are made at the readout stage using 2-qubit fusion measurements [31]. Central to our architecture is a specific resource state whose geometry is obtained by foliating [32,33] the Floquet color code [34,35]; an example of a dynamically driven code [36]. These codes are of recent interest due to their high thresholds [37,38] and their implementation with weight-two parity measurements. Our numerical simulations demonstrate very high thresholds by refining our architecture. Specifically, we propose using a decorated or “branched” one-dimensional cluster states to reduce the number of qubits we need to prepare and measure in the fault-tolerant system. In what follows, we describe our construction before presenting numerical results.

The foliated Floquet color code.—In measurement-based fault-tolerant quantum computation, we prepare a resource state that can be specified by a graph [23,39]. A qubit is initialized in an eigenstate of the Pauli- X matrix on every

Published by the American Physical Society under the terms of the Creative Commons Attribution 4.0 International license. Further distribution of this work must maintain attribution to the author(s) and the published article's title, journal citation, and DOI.

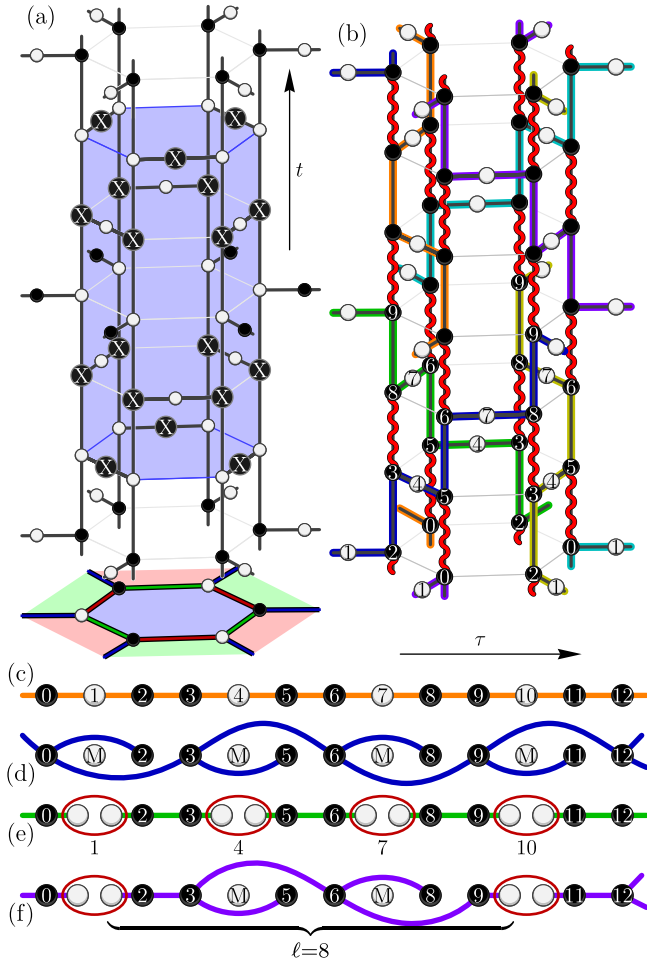


FIG. 1. Realizing the foliated Floquet color code with linear cluster states and fusion measurements. (a) The resource state \mathcal{R} we construct is illustrated by the graph. Detectors $S \in \mathcal{S} = \mathcal{R} \cap \mathcal{M}$ are the product of Pauli- X terms at the boundaries of local cells. The vertical timelike axis is labeled t , which indexes layers of the three-dimensional structure. (b) The resource state can be composed of one-dimensional cluster states, or “chains”, as in (c), shown by thick solid lines, and fusion measurements, marked by wavy red lines. The qubits of each chain are indexed with label τ . We can make variations of our construction with different input resources. We identify the qubits of the chain in (c) with those in (d)–(f) with their numerical indices. We obtain branched chains (d), up to local Clifford operations, by measuring white qubits of (c) in the Pauli- X basis. We can also produce long chains from small resource states by fusing the first and last qubit of linear chains of length $\ell = 4$, for example, (e). We can also fuse the end points of short branched chains (f), where we show a short branch of $\ell = 8$ qubits.

node of the graph v . Controlled-phase gates are then applied to pairs of qubits whose corresponding nodes share an edge. The stabilizer group [40] of the resource state \mathcal{R} is generated by elements $R_v = X_v \prod_{q \in \Delta v} Z_q$ for each node v , with Δv the neighborhood of v and X_v, Z_v the standard Pauli matrices acting on v . The resource is then measured, projecting it onto the state with stabilizer group \mathcal{M} ,

generated by the commuting Pauli measurements we make. The measurements provide syndrome data $\mathcal{S} = \mathcal{R} \cap \mathcal{M}$ that are used to identify errors [33,41,42]. We find our measurement-based model by foliating [32,33] the Floquet color code [34,35]. The resulting graph is shown in Fig. 1(a). We call our model the foliated Floquet color code (FFCC).

Foliation is a method for mapping circuit-based models, which are realized with static qubits, onto the measurement-based picture. Roughly speaking, data qubits of the static model are replaced with linear cluster states, where the ordering of the qubits of these linear clusters can be regarded as a timelike direction in the static picture. Measurements that are made in the static picture are realized in the measurement-based picture by coupling additional “check qubits” to the appropriate qubits of the linear clusters that model the time evolution of data qubits of the static model.

We obtain a three-dimensional lattice by applying the foliation methods described in Ref. [33] to the Floquet color code [34,35], where data qubits lie on vertices of a two-dimensional hexagonal lattice, shown at the base of Fig. 1(a). The graph describing \mathcal{R} has two types of nodes; let us call them data nodes and check nodes. Data nodes have indices (q, t) , where $1 \leq q \leq n$ index data qubits of the hexagonal lattice. The second index $1 \leq t \leq T$ denotes a temporal order. Data nodes (q, t) and $(q, t + 1)$ share an edge for all q and t .

The remaining edges to complete the graph for \mathcal{R} connect data nodes to check nodes. The check nodes are associated with the edges of the hexagonal lattice. There are three types of edges, which are assigned colors red, green, or blue [43]. Specifically, we three color the faces of the hexagonal lattice such that no two adjacent faces have the same color. Edges of the hexagonal lattice are then assigned the color of the two faces they connect. Let us also denote $\{v, w\} = \partial e$ as the pair of vertices of the hexagonal lattice that are connected by edge e . We have check nodes associated with edges of different colors at different times. Let us denote the check nodes with indices (e, t) . We have check nodes associated only with the blue, green, and red edges at times $3t + 1$, $3t + 2$, and $3t + 3$, respectively. Every check node (e, t) of the appropriate color then shares an edge with the two data nodes (v, t) for both $v \in \partial e$. These check nodes are entangled with the data nodes to correspond precisely to the measurement sequence of the Floquet color code according to the foliation methods of Ref. [33]. This completes the construction shown in Fig. 1(a).

Up to lattice geometry, the model we have produced shares many features with the topological cluster-state model [41] where, for now, we assume we measure all of the qubits in the Pauli- X basis; i.e., we project the system onto the stabilizer group $\mathcal{M} = \langle \pm X_v \rangle$ to obtain the code detectors that identify errors. The FFCC has local detectors $\mathcal{S} = \mathcal{R} \cap \mathcal{M}$ on cells of the lattice. We show an example of

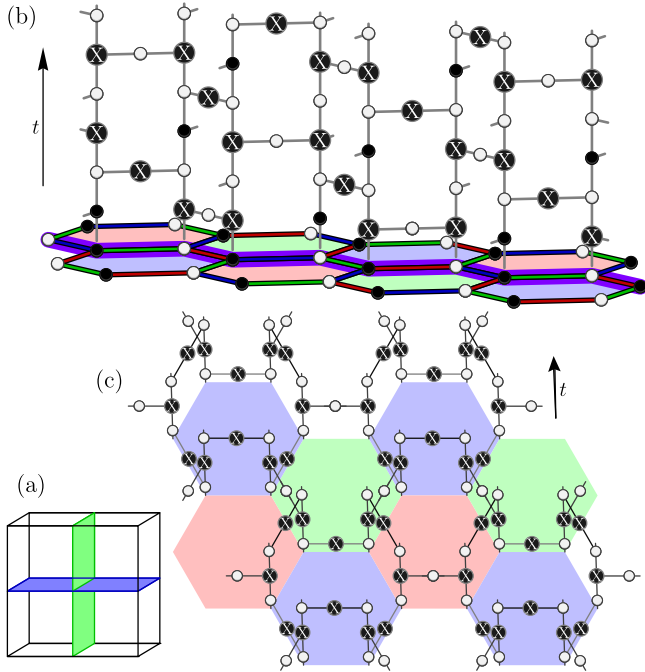


FIG. 2. Correlation surfaces in the foliated Floquet color code. (a) Shows the orientation of correlation surfaces that lie orthogonal to a canonical spatial direction and the temporal direction in green and blue, respectively. We show the microscopic details of these operators in (b) and (c), respectively, with timelike axes t marked with arrows.

a local detector in Fig. 1(a). Similarly, the foliated code gives rise to correlation surfaces that propagate quantum information between input and output regions [2,41,44]. We show examples of correlation surfaces in Fig. 2. Additionally, our model can be divided into two disjoint lattices of qubits: the primal and dual lattice, where detectors and correlation surfaces are supported on only one of the two disjoint lattices. The primal and dual lattices are distinguished with black and white vertices in Fig. 1(a) and Figs. 2(b) and 2(c).

The common features of our model with those in Ref. [41] mean that we can adopt the fault-tolerant gate set presented in Ref. [2] by reconfiguring our measurement pattern such that gates are performed by braiding different types of defect punctures and by distilling magic states to complete a universal gate set. It may be interesting to consider adapting the methods of Refs. [9,33,45,46] to our lattice geometry for more general gate operations based on the braiding of twist [47] and corner [33,48] defects. It may also be interesting to investigate implementations of non-Clifford gates with this lattice geometry [49,50].

Quantum computing with fusion measurements.—Let us now look for practical ways of preparing and measuring the resource state \mathcal{R} . Recently, Ref. [12] has shown that we can eliminate the difficulty of preparing a large entangled resource state by completing the preparation and readout of a resource state with probabilistic entangling Bell

measurements, i.e., fusion operations [31]. With an appropriate choice of fusion measurements, we find that we can decompose the graph shown in Fig. 1(a) into a series of physical one-dimensional cluster states, which we call chains, and fusion measurements only, see Fig. 1(b). The qubits of the chain are indexed $0 \leq \tau \leq 3T - 1$, see Fig. 1(c), where a single chain is laid out independent of the three-dimensional construction. In the figure, each chain is marked by bold lines of different colors, where we see that every chain has three qubits at each time step t .

It is helpful to bicolor the vertices of the hexagonal lattice black and white such that no two vertices of the same color share an edge. Likewise, data nodes (v, t) have the same color as vertex v of the hexagonal lattice. We identify all of the black qubits $(v, 1)$ of the foliated system at $t = 1$ with the $\tau = 0$ qubit of each chain. The next qubit of the chain with $\tau = 1$ is identified with the unique edge qubit $(e, 1)$ with $v \in \partial e$ and then qubit $\tau = 2$ is identified with $(w, 1) \neq (v, 1)$ with $w \in \partial e$. The chain then progresses to the next level before repeating, where the $\tau = 3$ element of the chain is identified with $(w, 2)$. The progression continues *ad infinitum*. In general, we have that the $\tau = 3t(3t + 1)$ th qubit lies at qubit (v, t) [(e, t) with $v \in \partial e$], and the $3t + 2$ th qubit of the chain lies at (w, t) and $w \in \partial e$ with $w \neq v$. The next qubit in each chain lies at qubit $(w, t + 1)$. Indices (v, t) and (w, t) are, respectively, black and white (white and black) for odd (even) values of t .

By comparing Figs. 1(a) and 1(b) we see the chains are organized such that many of the edges of the resource state graph are completed in the production of the chains. However, some entangling operations remain to be performed. We then complete the resource state with fusion operations. Up to local Clifford operations, we can interpret a successful fusion measurement as a controlled-phase gate, i.e., creation of an edge, followed by two single-qubit measurements in the Pauli- X basis. Fusion measurements shown in Fig. 1(b) therefore complete the entangling operations needed to produce the resource state and subsequently make the single-qubit measurements we need for readout. Specifically, we perform fusion measurements between black (white) data nodes (v, t) and $(v, t + 1)$ at odd (even) values of t . Final readout in single-qubit bases different from Pauli- X , required for universal gate sets, can also be simply implemented by reconfiguring the linear-optical fusion circuit used [7,12].

We consider variations where chains are replaced by other resources that may be more readily implemented. In Fig. 1(c) we show a single chain, where the data (check) nodes are marked black (white). As Fig. 1(b) shows, the check nodes are completely entangled with their neighbors ∂e when the chain is produced. We may therefore consider replacing the chain with a decorated chain that is the postmeasurement state that would be obtained if the check nodes of a standard chain are measured in the Pauli- X basis. Up to local Clifford operations [39] we obtain the resource

state with branches, as shown in Fig. 1(d). This state is readily prepared with quantum emitters, see Supplemental Material [51]. We call the measurement-based model realized with these decorated chains the “branched construction.” The branched construction therefore neglects to produce check nodes and only instead constructs the data nodes, such that the edge measurements are effectively already made.

We might also look for variations where we produce the large resource states from smaller entangled resources. For example, fusion measurements between qubits of $\ell = 4$ -qubit linear cluster states, as shown Fig. 1(e), produce the chains we use in our construction. We can also interpolate between the short chain construction and the branched chain construction by connecting finite-size branched chains at their end points via fusion measurements. We show a short branched chain of length $\ell = 8$ qubits in Fig. 1(f).

Error correction.—We can also adopt methods used for the topological cluster state to perform error-correction with the FFCC. We are interested in correcting Pauli errors as well as heralded qubit erasure occurring on the physical qubits of the system.

Every single qubit supports exactly two detectors [35]. It follows that, if a Pauli error occurs, two detectors are violated. We can therefore regard a single error as a string segment with violated detectors at its end points [1,41]. In general, multiple Pauli errors compound to make multiple strings of potentially greater length. We can correct the errors by finding pairs of violated detectors that are corrected by short string operators. Provided the proposed correction has an equal parity of errors supported on the correlation surface as the initial error, we declare the correction successful. We find nearby pairs of violated detectors using PyMatching [56], an implementation of minimum-weight perfect matching [1].

We also adopt the methods presented in Ref. [57] for dealing with heralded erasure. If a qubit v is erased, we no longer have access to its two stabilizers S_b and S_c that support v . To deal with this, we neglect the erased qubit, and we replace these two supporting stabilizers with their product $S_b S_c$, thereby creating a super cell. In general, we have to update the lattice to produce super cells for all the qubits that experience erasure. Error correction for Pauli errors on the updated lattice then proceeds in the same way using super cells on qubits that have not been erased. It is also important to find a correlation surface that contains no erased qubits. To do so, we multiply the correlation surface by detector operators to find a variation of the operator such that no qubits are erased. These can be readily achieved by Gaussian elimination [58]. Otherwise, we consider error correction to fail.

The error-correction methods described above are readily adapted for the fusion error model [12]. In this model, a fusion erasure takes into account the erasure of measured qubits as well as the possible failure of the fusion measurement.

The fusion error model also includes fusion measurement errors induced by Pauli errors on the fused qubits.

Threshold estimates.—We evaluate threshold error rates for a phenomenological fusion-based noise model as in Ref. [12] where erasures and errors occur independently for each fusion measurement and with a probability equal to the associated noise rate. Fusion networks are simulated with periodic boundaries so that we can check logical failures for the two distinct correlation surfaces shown on orthogonal planes in Fig. 2. Thresholds are evaluated by comparing the logical error rate of our decoder for different noise parameters and different lattice sizes. We evaluate logical failure rates with 10^4 Monte Carlo samples (see Supplemental Material [51] for details). We also report on an analysis for bare lattices in the Supplemental Material.

We show threshold error rates for different constructions in Fig. 3 for various rates of error and erasure that occur under fusion measurements. The highest thresholds are obtained using the branched chain construction. The threshold interpolates between an erasure rate $\sim 13.2\%$ to an error rate $\sim 1.5\%$. The thresholds we obtain outperform previous constructions based on hexagonal- and star-shaped resource states used to produce Raussendorf lattice structures [12]. We reproduced the thresholds for these models. They are shown by dashed and dotted lines in Fig. 3. Such improvements manifest the advantages of constructing a model with a lower valency lattice, a direct consequence of having only weight-two parity measurements, while still inheriting good error-correction performance of the underlying Floquet color code. The thresholds for constructions that include fusing branched chains of constant size, as shown in Figs. 1(e) and 1(f), are also reported in Fig. 3 for different lengths $\ell \in \{4, 8, 14\}$.

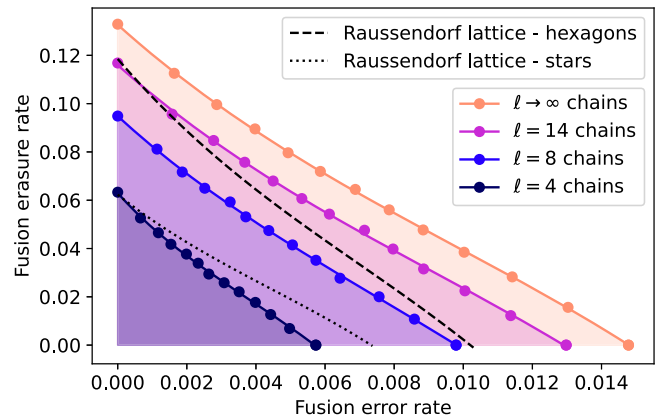


FIG. 3. Fault-tolerant regions for fusion-based constructions. Solid lines show thresholds when constructing the FFCC lattice by fusing branched chains with length $\ell \in \{4, 8, 14\}$ and for the limit $\ell \rightarrow \infty$ where the length is much longer than the lattice unit cell size. For comparison, we also show the performance of the constructions from Ref. [12] using hexagonal and 4-qubit star-shaped resource states by the dashed and dotted black lines, respectively.

Significant improvements over previous constructions can be observed already for chains with a moderate constant size of 14 qubits. Thresholds relative to erasure can also be significantly improved by biasing the fusion failures, as recently shown in Refs. [59,60]. In the Supplemental Material [51] we report how these techniques can enhance erasure thresholds also in our constructions.

Discussion.—To summarize, we have demonstrated a practical architecture to realize fault-tolerant measurement-based quantum computation using one-dimensional entangled resources. Such resource states are readily and deterministically prepared with quantum emitters, avoiding the large overheads required for preparing entangled resource states via multiplexed probabilistic processes in all-optical approaches [61] and can also be relevant for other physical systems with probabilistic entangling operations [62–64]. Furthermore, our numerical simulations demonstrate very high thresholds. We obtained these results focusing on phenomenological noise that models all noise sources with a single parameter. This allows us to compare our proposal with others already presented in the literature. In the future, it will be important to run simulations that consider more representative models of noise sources that we anticipate in the laboratory. In the Supplemental Material [51] we discuss some of them in the context of preparing linear cluster states with quantum emitters.

We argue that the high thresholds we have obtained are due to the resource efficient and practical construction we have designed that requires a relatively low number of fusion operations for its realization. Better models with higher noise tolerance could, perhaps, be obtained by finding more general lattice structures (see, e.g., Refs. [65,66]). Ultimately, we may find more robust models by finding more general resource states that can be readily produced, for example, with interactions between multiple emitters [22,67].

We are grateful for conversations with M. Löbl, L. Pettersson, A. Sørensen, and Y. Zhang. S. P. acknowledges funding from the Cisco University Research Program Fund (No. 2021-234494), the Marie Skłodowska-Curie Fellowship project QSun (No. 101063763), and the VILLUM FONDEN research grant (No. VIL50326). B. J. B. received support from the U.S. Department of Energy, Office of Science, National Quantum Information Science Research Centers, Codesign Center for Quantum Advantage (C2QA) under Award No. DE-SC0012704. This work is supported by the Novo Nordisk Foundation, Grant No. NNF22SA0081175, NNF Quantum Computing Programme. B. J. B. is grateful for the hospitality of the Center for Quantum Devices at the University of Copenhagen.

* stefano.paesani@nbi.ku.dk

[1] E. Dennis, A. Kitaev, A. Landahl, and J. Preskill, Topological quantum memory, *J. Math. Phys. (N.Y.)* **43**, 4452 (2002).

- [2] R. Raussendorf, J. Harrington, and K. Goyal, Topological fault-tolerance in cluster state quantum computation, *New J. Phys.* **9**, 199 (2007).
- [3] P. Shor, Fault-tolerant quantum computation, in *Proceedings of the 37th Conference on Foundations of Computer Science* (IEEE, 1996), pp. 56–65.
- [4] A. G. Fowler, M. Mariantoni, J. M. Martinis, and A. N. Cleland, Surface codes: Towards practical large-scale quantum computation, *Phys. Rev. A* **86**, 032324 (2012).
- [5] N. H. Nickerson, J. F. Fitzsimons, and S. C. Benjamin, Freely Scalable Quantum Technologies Using Cells of 5-to-50 Qubits with Very Lossy and Noisy Photonic Links, *Phys. Rev. X* **4**, 041041 (2014).
- [6] K. Nemoto, M. Trupke, S. J. Devitt, A. M. Stephens, B. Scharfenberger, K. Buczak, T. Nöbauer, M. S. Everitt, J. Schmiedmayer, and W. J. Munro, Photonic Architecture for Scalable Quantum Information Processing in Diamond, *Phys. Rev. X* **4**, 031022 (2014).
- [7] M. Gimeno-Segovia, P. Shadbolt, D. E. Browne, and T. Rudolph, From Three-Photon Greenberger-Horne-Zeilinger States to Ballistic Universal Quantum Computation, *Phys. Rev. Lett.* **115**, 020502 (2015).
- [8] B. Lekitsch, S. Weidt, A. G. Fowler, K. Mølmer, S. J. Devitt, C. Wunderlich, and W. K. Hensinger, Blueprint for a microwave trapped ion quantum computer, *Sci. Adv.* **3**, e1601540 (2017).
- [9] D. Herr, A. Paler, S. J. Devitt, and F. Nori, A local and scalable lattice renormalization method for ballistic quantum computation, *npj Quantum Inf.* **4**, 27 (2018).
- [10] C. Chamberland, G. Zhu, T. J. Yoder, J. B. Hertzberg, and A. W. Cross, Topological and Subsystem Codes on Low-Degree Graphs with Flag Qubits, *Phys. Rev. X* **10**, 011022 (2020).
- [11] A. S. Darmawan, B. J. Brown, A. L. Grimsmo, D. K. Tuckett, and S. Puri, Practical quantum error correction with the XZZX code and Kerr-cat qubits, *PRX Quantum* **2**, 030345 (2021).
- [12] S. Bartolucci, P. Birchall, H. Bombin, H. Cable, C. Dawson, M. Gimeno-Segovia, E. Johnston, K. Kieling, N. Nickerson, M. Pant *et al.*, Fusion-based quantum computation, [arXiv:2101.09310](https://arxiv.org/abs/2101.09310).
- [13] J. E. Bourassa, R. N. Alexander, M. Vasmer, A. Patil, I. Tzitrin, T. Matsuura, D. Su, B. Q. Baragiola, S. Guha, G. Dauphinais, K. K. Sabapathy, N. C. Menicucci, and I. Dhand, Blueprint for a scalable photonic fault-tolerant quantum computer, *Quantum* **5**, 392 (2021).
- [14] M. V. Larsen, C. Chamberland, K. Noh, J. S. Neergaard-Nielsen, and U. L. Andersen, Fault-tolerant continuous-variable measurement-based quantum computation architecture, *PRX Quantum* **2**, 030325 (2021).
- [15] K. Wan, S. Choi, I. H. Kim, N. Shutty, and P. Hayden, -Fault-tolerant qubit from a constant number of components, *PRX Quantum* **2**, 040345 (2021).
- [16] C. Chamberland, K. Noh, P. Arrangoiz-Arriola, E. T. Campbell, C. T. Hann, J. Iverson, H. Putterman, T. C. Bohdanowicz, S. T. Flammia, A. Keller, G. Refael, J. Preskill, L. Jiang, A. H. Safavi-Naeini, O. Painter, and F. G. S. L. Brandão, Building a fault-tolerant quantum computer using concatenated cat codes, *PRX Quantum* **3**, 010329 (2022).

- [17] J. Claes, J. E. Bourassa, and S. Puri, Tailored cluster states with high threshold under biased noise, *npj Quantum Inf.* **9**, 9 (2023).
- [18] A. Strikis and L. Berent, Quantum LDPC codes for modular architectures, *PRX Quantum* **4**, 020321 (2023).
- [19] R. Uppu, L. Midolo, X. Zhou, J. Carolan, and P. Lodahl, Quantum-dot-based deterministic photon–emitter interfaces for scalable photonic quantum technology, *Nat. Nanotechnol.* **16**, 1308 (2021).
- [20] C.-Y. Lu and J.-W. Pan, Quantum-dot single-photon sources for the quantum internet, *Nat. Nanotechnol.* **16**, 1294 (2021).
- [21] N. H. Lindner and T. Rudolph, Proposal for Pulsed On-Demand Sources of Photonic Cluster State Strings, *Phys. Rev. Lett.* **103**, 113602 (2009).
- [22] B. Li, S. E. Economou, and E. Barnes, Photonic resource state generation from a minimal number of quantum emitters, *npj Quantum Inf.* **8**, 11 (2022).
- [23] R. Raussendorf and H. J. Briegel, A One-Way Quantum Computer, *Phys. Rev. Lett.* **86**, 5188 (2001).
- [24] I. Schwartz, D. Cogan, E. R. Schmidgall, Y. Don, L. Gantz, O. Kenneth, N. H. Lindner, and D. Gershoni, Deterministic generation of a cluster state of entangled photons, *Science* **354**, 434 (2016).
- [25] D. Istrati, Y. Pilnyak, J. Loredó, C. Antón, N. Somaschi, P. Hilaire, H. Ollivier, M. Esmann, L. Cohen, L. Vidro *et al.*, Sequential generation of linear cluster states from a single photon emitter, *Nat. Commun.* **11**, 5501 (2020).
- [26] C.-W. Yang, Y. Yu, J. Li, B. Jing, X.-H. Bao, and J.-W. Pan, Sequential generation of multiphoton entanglement with a Rydberg superatom, *Nat. Photonics* **16**, 658 (2022).
- [27] P. Thomas, L. Ruscio, O. Morin, and G. Rempe, Efficient generation of entangled multi-photon graph states from a single atom, *Nature (London)* **608**, 677 (2022).
- [28] J.-C. Besse, K. Reuer, M. C. Collodo, A. Wulff, L. Wernli, A. Copetudo, D. Malz, P. Magnard, A. Akin, M. Gabureac, G. J. Norris, J. I. Cirac, A. Wallraff, and C. Eichler, Realizing a deterministic source of multipartite-entangled photonic qubits, *Nat. Commun.* **11**, 4877 (2020).
- [29] R. Vasconcelos, S. Reisenbauer, C. Salter, G. Wachter, D. Wirtitsch, J. Schmiedmayer, P. Walther, and M. Trupke, Scalable spin–photon entanglement by time-to-polarization conversion, *npj Quantum Inf.* **6**, 9 (2020).
- [30] R. Raussendorf, J. Harrington, and K. Goyal, A fault-tolerant one-way quantum computer, *Ann. Phys. (Amsterdam)* **321**, 2242 (2006).
- [31] D. E. Browne and T. Rudolph, Resource-Efficient Linear Optical Quantum Computation, *Phys. Rev. Lett.* **95**, 010501 (2005).
- [32] A. Bolt, G. Duclos-Cianci, D. Poulin, and T. M. Stace, Foliated Quantum Error-Correcting Codes, *Phys. Rev. Lett.* **117**, 070501 (2016).
- [33] B. J. Brown and S. Roberts, Universal fault-tolerant measurement-based quantum computation, *Phys. Rev. Res.* **2**, 033305 (2020).
- [34] M. Davydova, N. Tantivasadakarn, and S. Balasubramanian, Floquet codes without parent subsystem codes, *PRX Quantum* **4**, 020341 (2023).
- [35] M. S. Kesselring, J. C. M. de la Fuente, F. Thomsen, J. Eisert, S. D. Bartlett, and B. J. Brown, Anyon condensation and the color code, [arXiv:2212.00042](https://arxiv.org/abs/2212.00042).
- [36] M. B. Hastings and J. Haah, Dynamically generated logical qubits, *Quantum* **5**, 564 (2021).
- [37] C. Gidney, M. Newman, and M. McEwen, Benchmarking the planar honeycomb code, *Quantum* **6**, 813 (2022).
- [38] A. Paetznick, C. Knapp, N. Delfosse, B. Bauer, J. Haah, M. B. Hastings, and M. P. da Silva, Performance of planar Floquet codes with Majorana-based qubits, *PRX Quantum* **4**, 010310 (2023).
- [39] M. Hein, W. Dür, J. Eisert, R. Raussendorf, M. Nest, and H.-J. Briegel, Entanglement in graph states and its applications, [arXiv:quant-ph/0602096](https://arxiv.org/abs/quant-ph/0602096).
- [40] D. Gottesman, Stabilizer codes and quantum error correction, Ph.D. thesis, California Institute of Technology, 2001.
- [41] R. Raussendorf, S. Bravyi, and J. Harrington, Long-range quantum entanglement in noisy cluster states, *Phys. Rev. A* **71**, 062313 (2005).
- [42] T. J. Bell, L. A. Pettersson, and S. Paesani, Optimising graph codes for measurement-based loss tolerance, [arXiv:2212.04834v1](https://arxiv.org/abs/2212.04834v1).
- [43] H. Bombin and M. A. Martin-Delgado, Topological Quantum Distillation, *Phys. Rev. Lett.* **97**, 180501 (2006).
- [44] R. Raussendorf, D. E. Browne, and H. J. Briegel, Measurement-based quantum computation on cluster states, *Phys. Rev. A* **68**, 022312 (2003).
- [45] D. Herr, A. Paler, S. J. Devitt, and F. Nori, Lattice surgery on the Raussendorf lattice, *Quantum Sci. Technol.* **3**, 035011 (2018).
- [46] H. Bombin, C. Dawson, R. V. Mishmash, N. Nickerson, F. Pastawski, and S. Roberts, Logical blocks for fault-tolerant topological quantum computation, *PRX Quantum* **4**, 020303 (2023).
- [47] H. Bombin, Topological Order with a Twist: Ising Anyons from an Abelian Model, *Phys. Rev. Lett.* **105**, 030403 (2010).
- [48] B. J. Brown, K. Laubscher, M. S. Kesselring, and J. R. Wootton, Poking Holes and Cutting Corners to Achieve Clifford Gates with the Surface Code, *Phys. Rev. X* **7**, 021029 (2017).
- [49] H. Bombin, 2D quantum computation with 3D topological codes, [arXiv:1810.09571](https://arxiv.org/abs/1810.09571).
- [50] B. J. Brown, A fault-tolerant non-Clifford gate for the surface code in two dimensions, *Sci. Adv.* **6**, eaay4929 (2020).
- [51] See Supplemental Material at <http://link.aps.org/supplemental/10.1103/PhysRevLett.131.120603> for additional details on the resource states considered, the analysis methods, and additional techniques to improve the fault-tolerance thresholds, which includes Refs. [52–56].
- [52] <https://github.com/StefanoPaesani/FusionLattices>.
- [53] J. P. Bonilla Ataides, D. K. Tuckett, S. D. Bartlett, S. T. Flammia, and B. J. Brown, The XZZX surface code, *Nat. Commun.* **12**, 2172 (2021).
- [54] W. P. Grice, Arbitrarily complete Bell-state measurement using only linear optical elements, *Phys. Rev. A* **84**, 042331 (2011).
- [55] J. M. Auger, H. Anwar, M. Gimeno-Segovia, T. M. Stace, and D. E. Browne, Fault-tolerant quantum computation with nondeterministic entangling gates, *Phys. Rev. A* **97**, 030301(R) (2018).
- [56] O. Higgott, pyMatching: A PYTHON package for decoding quantum codes with minimum-weight perfect matching, *ACM Trans. Quantum Comput.* **3**, 1 (2022).

- [57] S. D. Barrett and T. M. Stace, Fault Tolerant Quantum Computation with Very High Threshold for Loss Errors, *Phys. Rev. Lett.* **105**, 200502 (2010).
- [58] N. Connolly, V. Londe, A. Leverrier, and N. Delfosse, Fast erasure decoder for a class of quantum LDPC codes, [arXiv:2208.01002](https://arxiv.org/abs/2208.01002).
- [59] K. Sahay, J. Claes, and S. Puri, companion Letter, Tailoring fusion-based error correction for high thresholds to biased fusion failures, *Phys. Rev. Lett.* **131**, 120604 (2023).
- [60] H. Bombín, C. Dawson, N. Nickerson, M. Pant, and J. Sullivan, Increasing error tolerance in quantum computers with dynamic bias arrangement, [arXiv:2303.16122](https://arxiv.org/abs/2303.16122).
- [61] S. Bartolucci, P. Birchall, D. Bonneau, H. Cable, M. Gimeno-Segovia, K. Kieling, N. Nickerson, T. Rudolph, and C. Sparrow, Switch networks for photonic fusion-based quantum computing, [arXiv:2109.13760](https://arxiv.org/abs/2109.13760).
- [62] C. Monroe, R. Raussendorf, A. Ruthven, K. R. Brown, P. Maunz, L.-M. Duan, and J. Kim, Large-scale modular quantum-computer architecture with atomic memory and photonic interconnects, *Phys. Rev. A* **89**, 022317 (2014).
- [63] N. Roch, M. E. Schwartz, F. Motzoi, C. Macklin, R. Vijay, A. W. Eddins, A. N. Korotkov, K. B. Whaley, M. Sarovar, and I. Siddiqi, Observation of Measurement-Induced Entanglement and Quantum Trajectories of Remote Superconducting Qubits, *Phys. Rev. Lett.* **112**, 170501 (2014).
- [64] M. Ruf, N. H. Wan, H. Choi, D. Englund, and R. Hanson, Quantum networks based on color centers in diamond, *J. Appl. Phys.* **130**, 070901 (2021).
- [65] N. Nickerson and H. Bombín, Measurement based fault tolerance beyond foliation, [arXiv:1810.09621](https://arxiv.org/abs/1810.09621).
- [66] M. Newman, L. A. de Castro, and K. R. Brown, Generating fault-tolerant cluster states from crystal structures, *Quantum* **4**, 295 (2020).
- [67] M. Gimeno-Segovia, T. Rudolph, and S. E. Economou, Deterministic Generation of Large-Scale Entangled Photonic Cluster State from Interacting Solid State Emitters, *Phys. Rev. Lett.* **123**, 070501 (2019).